ELSEVIER

Chemical Engineering Journal 88 (2002) 187–200

Chemical Engineering Journal

www.elsevier.com/locate/cej

Incorporating zeolites in microchemical systems

Joseph Lik Hang Chau [a], Yu Shan Susanna Wan [a], Asterios Gavriilidis [b], King Lun Yeung [a,*]

[a] *Department of Chemical Engineering, The Hong Kong University of Science and Technology, Clear Water Bay, Kowloon, Hong Kong*
[b] *Department of Chemical Engineering, University College, London, Torrington Place, London WC1E 7JE, UK*

Received 18 May 2001; accepted 16 October 2001

Abstract

Using a new fabrication method based on microelectronic fabrication and zeolite thin film technologies, MFI-type zeolites with engineered structures were incorporated as catalyst, membrane and structural material within the design architecture of a microreactor, membrane microseparator and microeletrochemical cell. Complex microchannel geometry and network (<5 μm), as well as zeolite arrays (<10 μm) were successfully fabricated onto highly orientated supported zeolite films. The zeolite micropatterns were stable even after repeated thermal cycling between 303 and 873 K for prolonged period of time. Blueprints for zeolite-based microchemical systems were presented, and test units were fabricated and the structural details of the microdevices' architecture were analysed.

Keywords: Microchemical system; MEMS; Microreactor; Microseparator; Zeolite and MFI

1. Introduction

Zeolites are microporous tectosilicate crystals with uniform nanometer-sized pores. The pore structure of the zeolite restricts the size and shape of the molecules that can enter and leave the channels. This gives rise to molecular sieving effects observed in many separation and reaction processes involving zeolites [1]. Unlike the most microporous metal oxides (e.g., SiO_2, Al_2O_3 and TiO_2) which have tortuous pore channels, zeolites have a well-defined pore system and a crystalline structure. The chemical environment within the zeolite pore channel can be manipulated to influence the molecular transport of diffusing species during separation. In addition, its unique framework chemistry and high internal surface area offer an excellent catalytic environment for many chemical reactions. Besides their applications in petrochemical production [2], zeolites can be employed in the synthesis of fine chemicals and pharmaceuticals [3–5], in pollution abatement [5,6], in membranes [7], in membrane reactors [8,9], in sensors [10–13], and in optoelectronic materials [14]. More recently, Wan et al. [15] outlined several fabrication methods for zeolite-based microreactor and membrane microseparator. These belong to an emerging new technology: the microchemical systems that also include other microdevices such as micromixers, microheat exchangers, microactuators and microsensors [16]. Ultimately, these discrete components can be assembled to create microanalytical laboratories, portable manufacturing plants and miniature fuel cells to satisfy the needs of an increasingly mobile society.

Microreactors have great potential as analytical tools for catalytic, chemical and biochemical research. They also represent another method for production of speciality chemicals and biochemicals. Their unique properties, which include high heat and mass transfer rates [17–22] and short residence time [23] make them an invaluable tool for studying demanding reaction systems. Microreactors can provide important information on reaction mechanisms and intrinsic kinetic rates that are essential for reactor design and scale-up. They can also be used for rapid screening of synthesis pathways to determine the most efficient and environmentally responsible synthesis route. Pioneering work in microreactor has been carried out among others by groups at Institüt für Mikrotechnik Mainz (IMM), Forschungszentrum Karlsruhe GmbH (FK), Massachusetts Institute of Technology (MIT), Pacific Northwest National Laboratory (PNNL), Technische Universität Chemnitz (TUC), etc.

Miniaturisation can also benefits membrane separation processes. It enables large membrane area to be accommodated within a small volume allowing for the design of a compact separation unit. Instead of one continous membrane

* Corresponding author. Tel.: +852-2358-7123; fax: +852-2358-0054.
E-mail address: kekyeung@ust.hk (K.L. Yeung).

1385-8947/02/$ – see front matter
PII: S1385-8947(01)00287-X

surface, a membrane microseparator will consist of an assembly of smaller membranes that provides the same effective separation area. It is expected that by keeping the individual membranes' area small, the risk of membrane failure due to accumulated stresses can be significantly diminished. This is particularly important for inorganic membranes, where embrittlement, crack formation and delamination are some of the leading causes of failure. An early attempt to built a membrane microseparator has been described by Ehrfeld et al. [24]. Franz et al. [25] reported a palladium membrane microseparator for hydrogen-based separations and reactions. den Exter et al. [26] and Wan et al. [15] prepared free-standing zeolite micromembranes on silicon substrates.

Unlike the integrated circuit (IC) industry that have adopted a single production standard (i.e., complementary metal oxide semiconductor (CMOS) technology), microelectromechanical and microchemical systems have multiple fabrication and assembly processes [27,28]. These include traditional semiconductor fabrication technology [29], LIGA [30,31], multi-lamination [32,33], laser micromachining [34,35], and dip pen nanolithography [36]. Thin zeolite films can be grown on planar supports using hydrothermal synthesis, with or without prior seeding [37,38]. More recently, Yoon and co-workers [39] created 100 μm range patterns through adhesion of zeolite powders onto micropatterned polyelectrolyte layer. In this work, we employ traditional semiconductor fabrication methodology along with zeolite thin film technology to create microstructured patterns that can be employed in microchemical systems, such as microreactors, microseparators or microelectrochemical cells.

2. Experimental

Fig. 1 gives the general outline of the procedure for the fabrication of zeolite-based microstructured patterns using standard semiconductor microfabrication technology. First, a zeolite–silicon composite was prepared by growing oriented polycrystalline zeolite film onto a silicon wafer. The design pattern was then transferred and etched onto the zeolite–silicon composite using conventional photolithography.

2.1. Preparation and fabrication of zeolite–silicon composite substrate

Two different approaches were employed in this study to prepare well intergrown, polycrystalline zeolite films onto silicon substrates (4 in. diameter p-type Si(1 0 0)). In the first method (Fig. 1A and C), silicalite-1 (Sil-1) films on silicon were prepared from a synthesis mixture containing 6.5 ml of organosilicon precursor, tetraethyl orthosilicate (TEOS, 98%, Aldrich) mixed with 65 ml of 0.05 M aqueous solution of the organic template, tetrapropylammonium hydroxide (TPAOH, 1 M, Aldrich) to give mole ratios of 80 TEOS:10 TPAOH:10,000 H_2O. The silicon was held in a horizontal position with the polished surface facing downwards. This decreased the number of growth defects caused by incorporation of zeolite powder from the solution. The backside of the silicon was covered with a layer of Teflon ribbon to prevent zeolite growth. Placed within an autoclave vessel, the completely immersed silicon was hydrothermally treated at 448 K in a preheated oven (Memmert) between 6 and 48 h.

In the second approach (Fig. 1B and C), the silicon substrate was pre-seeded with zeolite nanocrystals before hydrothermal synthesis. Sterte et al. [40] have shown that submicron MFI zeolite films can be successfully grown onto seeded silicon. The colloidal Sil-1 seeds used in this study were prepared using the procedure described in a previous work [41]. The seeding procedure involved immersion of the silicon in 0.05 M 3-mercaptopropyl trimethoxysilane (99%, Aldrich)/ethanol solution in order to functionalise the substrate. The excess surfactants were rinsed off using ethanol. This was followed by immersion in colloidal suspension of Sil-1 seeds. The seeded substrate was then dried in the oven at 333 K for 15 min. This procedure gave uniform seed coverage on the silicon. The seed population on the substrates can be adjusted by repeating the seeding process several times. This way, seed populations up to 95×10^{12} crystals/m^2 (i.e., complete surface coverage) were obtained. The seeded silicon was then placed horizontally in a synthesis mixture containing 40 TEOS:10 TPAOH:20,000 H_2O, and sealed in an autoclave for hydrothermal regrowth at 398 K. Zeolite films grown for 12, 24, 48 and 72 h were examined to determine layer thickness, surface morphology and film orientation. After the synthesis, the zeolite–silicon composites were rinsed in deionised distilled water, dried overnight in an oven at 333 K and stored in a dry container (Fig. 1D).

Starting with a zeolite–silicon composite substrate, a new fabrication protocol was established. A 2.5 μm thick layer of positive photoresist (HPR-206, Fuji-Hunt Electronics Technology) was spin-coated onto the substrate (Fig. 1E). The resist was soft baked at 383 K for 1 min. Using contact printing, the micropattern etched on the photomask was transferred onto the polymer resist layer after exposure to UV light (Fig. 1F). The resist irradiated with UV light was washed away using FHD-5 positive developer (Olin) to expose the zeolite layer underneath (Fig. 1G). The sample was then hard baked at 393 K for 30 min to harden the photoresist and improve its adhesion. A buffered oxide etching solution (Superwet BOE Etchant 6-1, General Chemical) containing 1 HF:6 NH_4F was used to isotropically etch the micropattern onto the zeolite layer (Fig. 1H). The etched substrate was rinsed with deionised distilled water and dried using clean nitrogen gas. The photoresist was stripped from the surface using acetone (Fig. 1I). After a final rinse in deionised distilled water, the patterned substrate was dried overnight at 333 K and calcined in air at 823 K for 6 h to remove the organic templates trapped within the zeolite cages. This final step frees the zeolite pore environment for catalysis and separation.

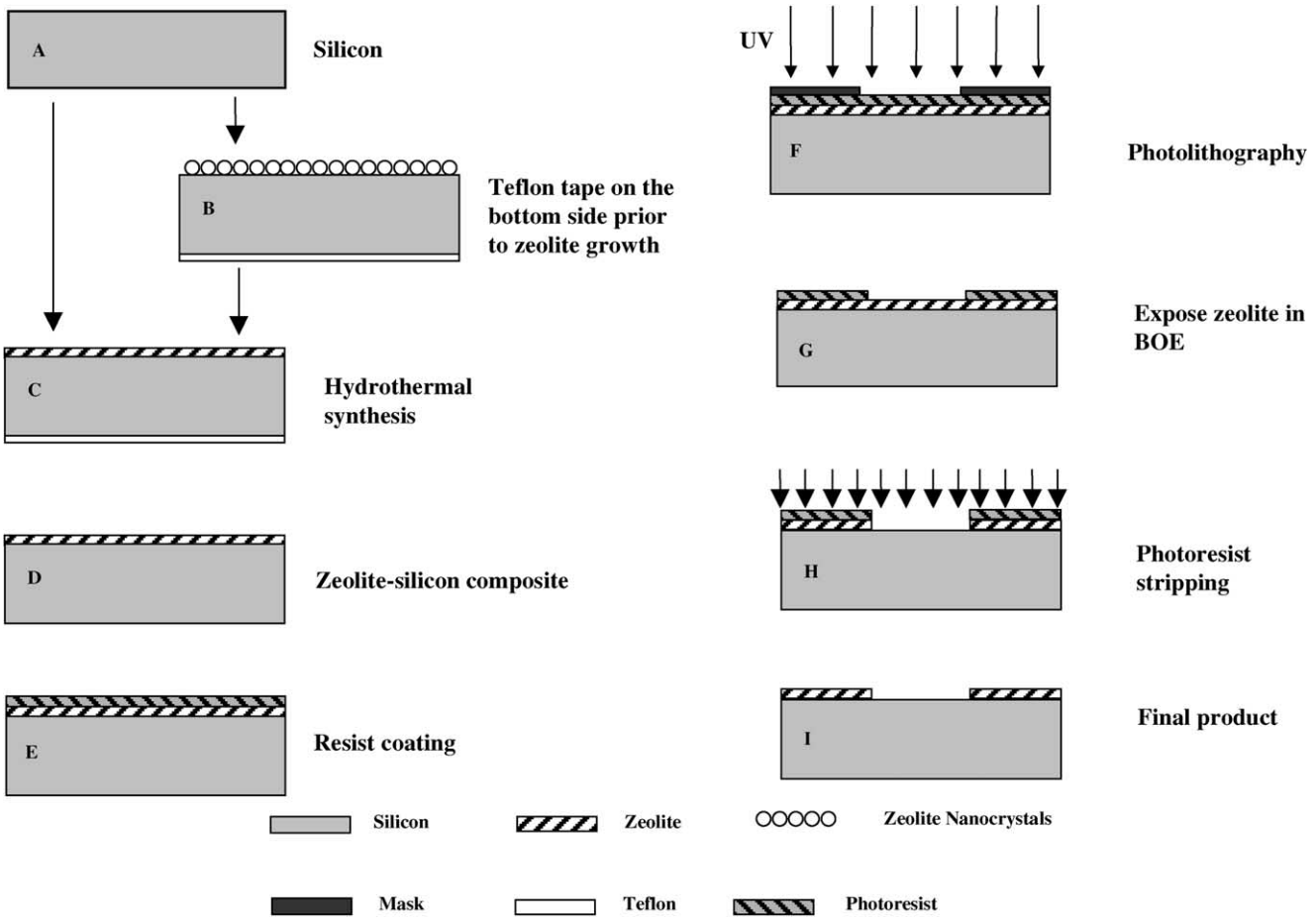

Fig. 1. Process diagram for fabrication of zeolite-based micropatterns.

2.2. Characterisation

Structural analyses were conducted using X-ray diffraction (XRD) and scanning electron microscopy (SEM). The crystal structure, crystallinity and crystallographic orientation of the zeolite film were determined using a Philips PW 1030 X-ray diffractometer equipped with Cu Kα X-ray source and graphite monochromator. The X-ray line intensity was obtained for $5^\circ \leq 2\theta \leq 45^\circ$ at a scan rate of 0.02°/min and time constant of 0.02. The film thickness, grain size and zeolite morphology were examined using a JEOL JSM 6300 scanning electron microscope. The samples were mounted onto aluminium specimen stubs with conducting carbon tape and sputter-coated with a 10 nm layer of gold to reduce sample charging. The samples at various stages of fabrication were inspected visually using an optical microscope (Olympus, BH-2). The surface roughness of the silicon substrate was examined by atomic force microscopy (Nanoscope IIIα, Digital Instruments). These combined characterisation techniques provide a detailed information on the microstructure of the zeolite–silicon composite material used in the preparation of microchemical devices.

3. Results and discussions

3.1. Preparation of zeolite–silicon composite

The clean silicon substrate (Fig. 2a) was seeded using the procedure described in Section 2 in order to obtain a complete and uniform seed coverage (i.e., 95×10^{12} seeds/m^2) as shown in Fig. 2b. The 120 nm colloidal Sil-1 seeds were roughly ellipsoidal in shape with no apparent crystal facets. XRD analysis of the zeolite seeds indicated an MFI-type crystalline structure. It was clear from comparing the surface line profiles of the plain (Fig. 2a, inset) and seeded silicon (Fig. 2b, inset) obtained by atomic force microscope that seeding results in an increased surface roughness.

The deposition and growth of Sil-1 zeolite onto clean and seeded silicon substrates are shown in Figs. 3 and 5, respectively. Fig. 3 displays the microstructure of Sil-1 zeolite deposited onto silicon substrate after 6, 12, 24 and 48 h of hydrothermal synthesis. Approximately 4.7×10^9 crystals/m^2 occupied the surface of the sample after 6 h of synthesis (Fig. 3a). The zeolites had a relatively uniform size of $7\,\mu m \times 17\,\mu m$ giving the crystals an average length-to-width

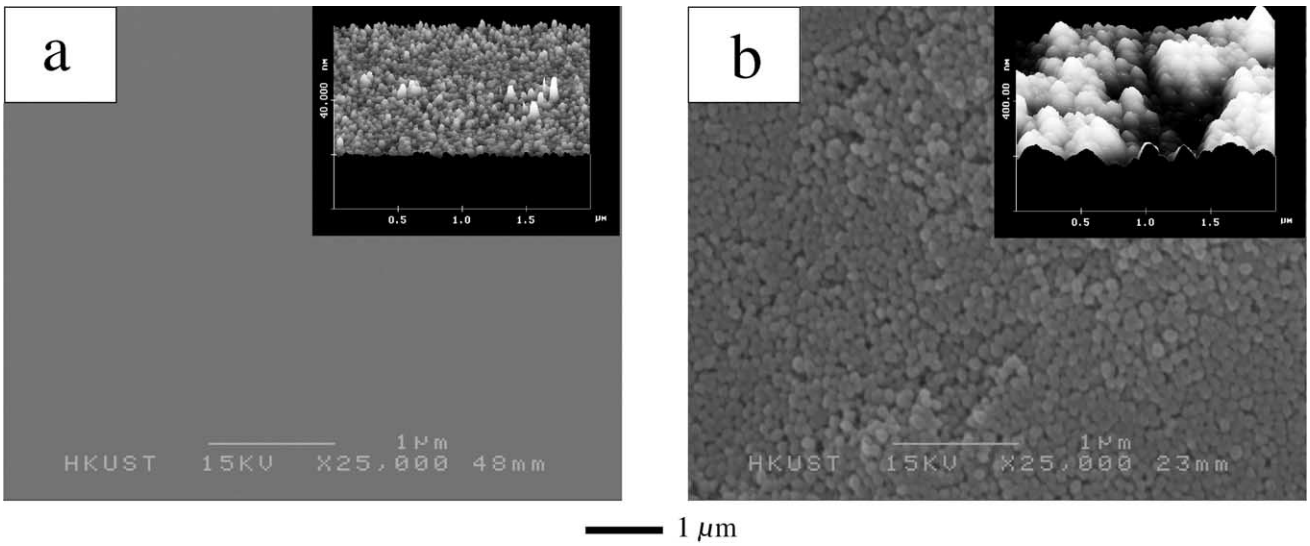

Fig. 2. Scanning electron and atomic force micrographs of: (a) plain silicon and (b) seeded silicon substrates (figure insets are AFM surface profiles of the plain and seeded silicons at the same magnification).

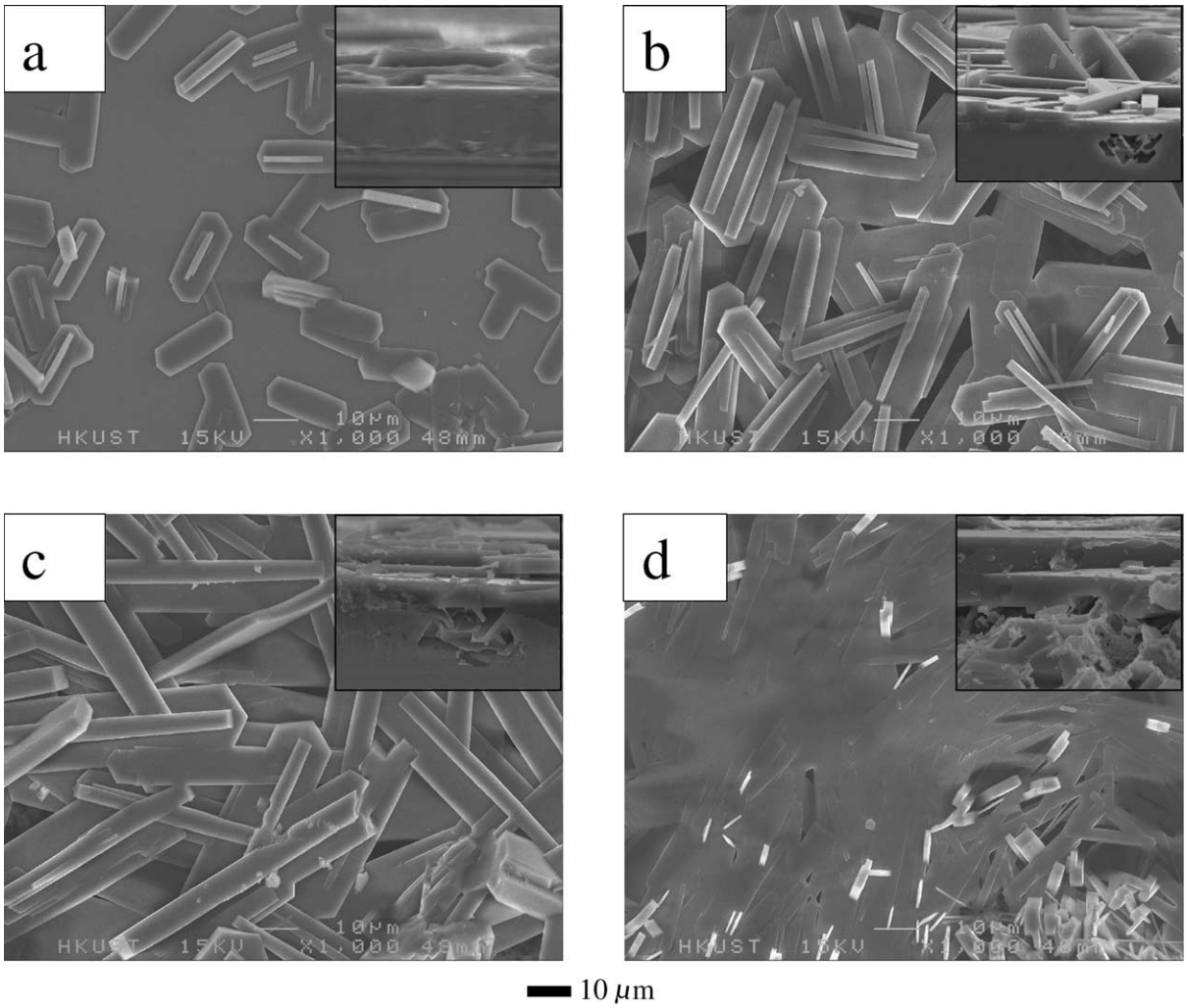

Fig. 3. Scanning electron micrographs of Sil-1 grown on plain silicon for: (a) 6 h, (b) 12 h, (c) 24 h and (d) 48 h of hydrothermal synthesis [80 TEOS:10 TPAOH:10,000 H_2O, 448 K] (figure insets are the cross-sectional views at 2.5× higher magnification).

ratio of 2.4. The coffin-shaped crystals had a thickness of about 2.3 μm (Fig. 3a, inset). Intergrowth and coalescence were evident where two neighbouring crystals impinged upon one another, forming larger irregular shaped rafts. Although the individual zeolites had random placement and alignment on the silicon surface, most of the crystals grew on the silicon with their (0 2 0) plane parallel to the surface. This means that the straight zeolite pore channels were aligned perpendicular to the surface. About half of the crystals exhibited secondary growths that emerge from the flat (0 2 0) planes. These secondary crystals were oriented with their (2 0 0) planes parallel to the silicon surface. The resulting morphology was reminiscence of twinned Sil-1 crystals. The inset in Fig. 3a shows that the surface of the zeolite–silicon composite substrate is rough, mainly because of the nonuniform coating and presence of secondary growths.

Through crystal growth and coalescence, nearly 90% of the surface was covered by zeolite crystals after 12 h of synthesis (Fig. 3b). Further nucleation was not evident and the crystal population per unit area remained unchanged. The crystals were significantly larger (9 μm × 32 μm) with most of the growth along their length (i.e., *c*-axis). This resulted in an elongated shape with a length-to-width ratio of 3.7. Growth along the zeolite width (i.e., *a*-axis) and thickness (i.e., *b*-axis) were small in comparison. Secondary in-plane (Fig. 3b) and off-plane crystal growths (Fig. 3b, inset) were common. This resulted in an uneven surface as shown in the inset of the figure. It is interesting to note that cavities formed by dissolution of the silicon substrate were also observed. Usually the cavities were hidden beneath the zeolite layer, and were therefore undetectable from surface inspection. After 24 h of hydrothermal synthesis (Fig. 3c), the crystals nearly doubled in size compared to those shown in Fig. 3b. These zeolites were roughly 6 μm thick, 16 μm wide and 64 μm long. Nearly all crystals exhibited secondary growth, which was responsible for its rough surface (Fig. 3c, inset). An additional 24 h of synthesis allowed the secondary crystals with (2 0 0) orientation to grow sufficiently large to coalesce and form an intergrown layer (Fig. 3d). Imperfections in the form of misaligned crystals interrupted the otherwise smooth surface (Fig. 3d). Unfortunately, defects in the form of large cavities within the silicon were also present (Fig. 3d, inset). The XRD pattern of this zeolite–silicon composite is shown in Fig. 4a.

Without pre-seeding, zeolite nuclei were formed on silicon by heterogeneous nucleation or were incorporated after it had nucleated in the solution (i.e., homogeneous nucleation). It had also been suggested that microcrystals deposited from the solution may act as seeds for zeolite growth [42]. The number of nuclei formed was usually less than 1 μm^{-2}, especially in the absence of ageing. This means that the concentration of nutrients immediately surrounding the seeds is uniform. Off-plane crystal growth was observed (Fig. 3b, inset), but were not as common as the in-plane zeolite growth (Fig. 3a). The latter zeolites were oriented with their (0 2 0) plane parallel to the surface. It had been argued that the (0 2 0)-oriented zeolite crystals have a more stable configuration because of their larger contact area with the support [37]. These zeolite crystals displayed anisotropic growth that was typical of MFI zeolite [43,44]. The growth rate along the *c*-axis of the zeolite crystal (i.e., ⟨0 0 2⟩) was the highest at 2.6 μm/h, followed by *a*-axis (i.e., ⟨2 0 0⟩) at 0.6 μm/h and *b*-axis (i.e., ⟨0 2 0⟩) at 0.2 μm/h. This means that the zeolite grew rapidly along the support surface resulting in a complete coverage at less than 24 h of synthesis, but the growth along the layer thickness corresponding to the zeolites' *b*-axis is small. A competing crystal orientation was evident even at the start of film growth (Fig. 3a). The (2 0 0)-oriented crystals grew directly from the existing (0 2 0) crystals, and predominated once the (0 2 0) crystals formed a complete film. This gave the resulting zeolite film (Fig. 3d) two distinct layers of different crystallographic orientations.

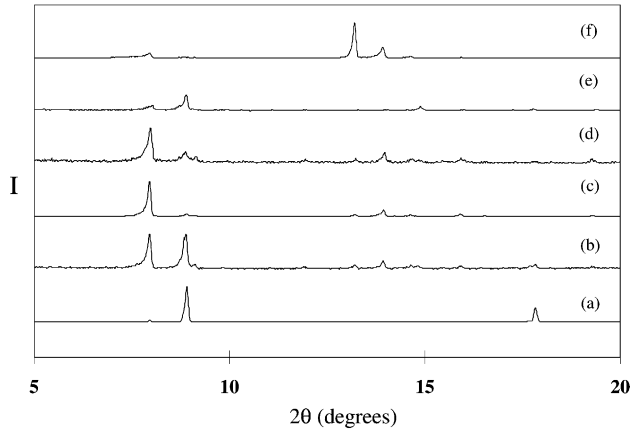

Fig. 4. XRD patterns of samples shown in (a) Fig. 3d, (b) Fig. 6a, (c) Fig. 6b, (d) Fig. 5c, (e) Fig. 7a and (f) Fig. 7b.

A (0 2 0)-oriented Sil-1 film, with its straight pore channels, is of great interest in membrane separation, and the slow crystal growth along the *b*-axis is ideal for the preparation of ultrathin zeolite membranes. However, the rough film surface and presence of microcavities mean that fabrication of defect-free, high-resolution micropatterns is difficult. Also, most microchemical systems will require high-aspect ratio patterns that demand a thick zeolite layer. In these circumstances, a film consisting of zeolites oriented along its *c*- or *a*-axis (i.e., faster growth rate) are more appropriate. Fig. 5 shows the zeolite microstructure grown on seeded silicon for 12, 24, 48 and 72 h. Unlike the zeolites grown on plain silicon, a complete film was obtained after 12 h of hydrothermal synthesis (Fig. 5a). The 1.1 μm thick zeolite layer consisted of intergrown crystals (Fig. 5a, inset). The zeolites were aligned with their *c*-axis nearly normal to the surface. XRD analysis indicated that the zeolites grew with a preferred orientation of (1 0 1) on seeded silicon (Fig. 4d). Analysis of the SEM images indicated that the grains had an average size of 0.6 μm and a length-to-width ratio of 1.4. These gave the grains a rectangular shape as shown in

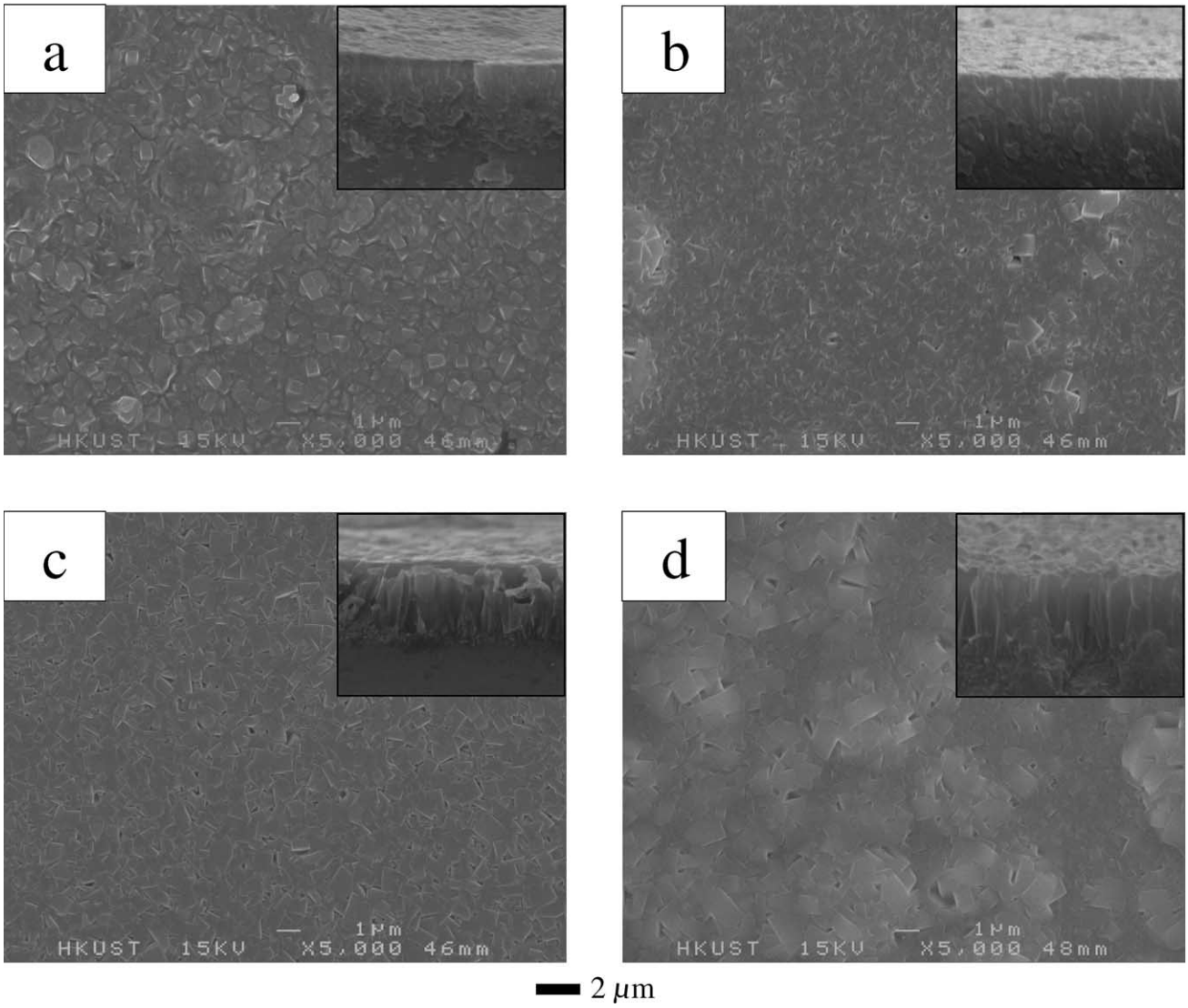

Fig. 5. Scanning electron micrographs of Sil-1 grown on silicon with 95×10^{12} seeds/m^2 for: (a) 12 h, (b) 24 h, (c) 48 h and (d) 72 h of hydrothermal synthesis [40 TEOS:10 TPAOH:20,000 H_2O, 398 K] (figure insets are the cross-sectional views at 2× higher magnification).

Fig. 5a. Zeolite films grown for longer time (i.e., 24–72 h) had larger crystal grain size, better intergrowth and smoother film surface as shown in Fig. 5b–d. Through growth and coalescence with neighbouring crystals, the grain size increases from 0.6 to 1, 1.3 and 2.3 μm, whereas the film thickness increases from 1.1 to 2.2, 2.9 and 4.1 μm after 12, 24, 48 and 72 h of synthesis, respectively. As a result, the individual zeolite crystals had a wedge-like shape (cf. Fig. 5c, inset). Due to the extensive coalescence and intergrowth between the crystals, it was difficult to ascertain the grain morphology from the SEM images. However, it is clear from the figures that the intercrystal grain boundary decreases with the synthesis time. XRD analysis indicated that these zeolite films have a (1 0 1)-preferred orientation (Fig. 4d).

The zeolite nanocrystals on the seeded silicon acted as nuclei for zeolite crystal growth. From the seed layer, the zeolites grew towards the solution where the concentration of the nutrient is high. Coalescence and growth termination were the results of the intense competition between neighbouring growing crystals, and helped shape the film microstructure. The dense crystal population and the relatively uniform concentration gradient of nutrient above the growing zeolite layer favoured the growth of the crystal along the *c*-axis. This gave the MFI zeolite film a preferred (1 0 1) orientation. The intergrowths between neighbouring crystals provided the polycrystalline film its mechanical strength and stability. The zeolite films (Fig. 5) grown from a seed layer and dilute synthesis solution do not display any abscess or microcavity defects as observed in Fig. 3b–d. However, the growth rate was slow with the growth along the *c*-axis at only about 0.14 μm/h, while the *b*- and *c*-axes were approximately 0.05 μm/h. Higher growth rates can be obtained by using more concentrated synthesis mixtures and higher hydrothermal treatment temperatures.

Fig. 6 shows the Sil-1 film microstructures obtained from two different seed concentrations. Fig. 6a displays the zeolite film grown on silicon with seed population of about 1.5×10^{12} seeds/m^2 (i.e., 1.5 seed/μm^2) which is about 1.6% of complete seed coverage. The 2 μm thick polycrystalline film was made of randomly oriented intergrown zeolite crystals as shown in the figure. This was confirmed by the XRD pattern in Fig. 4b. Diffraction peaks corresponding to (1 0 1) and (2 0 0)/(0 2 0) crystallographic orientations were evident in the figure. Zeolites grown on silicon wafer with a partial seed coverage ($\sim$26%) of 25×10^{12} seeds/m^2 formed a polycrystalline film (Fig. 6b) with (1 0 1) orientation (Fig. 4c). Fig. 6b shows that the zeolite film was 4 μm thick with an average grain size of 1.4 μm. Examination of the XRD patterns shown in Fig. 4a–d indicates that zeolite film orientation is influenced by the initial seed population present on silicon. Zeolite grown on unseeded substrate had predominantly (0 2 0) and (2 0 0) orientations (Fig. 4a). The additions of zeolite seeds favoured the growth of film with (1 0 1) orientations (Fig. 4b–d). As the seed population increases to full coverage, a well-oriented (1 0 1) zeolite film was obtained (Fig. 4d). Intermediate seed coverages led to films with mixed (1 0 1) and (2 0 0)/(0 2 0) orientations. This suggests that the zeolite film orientation can be manipulated through seeding. Changing the seed population alters the immediate environment of the growing zeolite. Growth competition between neighbours can significantly change the concentration gradient of nutrients around the growing crystal and can affect the growth of the zeolite [44].

Fig. 6c and d displays two additional film orientations obtained by changing the composition of the synthesis mixture. A (2 0 0)-oriented zeolite film (Fig. 6c) was grown on silicon from a synthesis solution containing boric acid. Early work of Jansen [43] has shown that boron preferentially inhibits the zeolite growth (ZSM-5) along the *c*-axis. This enabled the growth of the *a*-axis to predominate giving

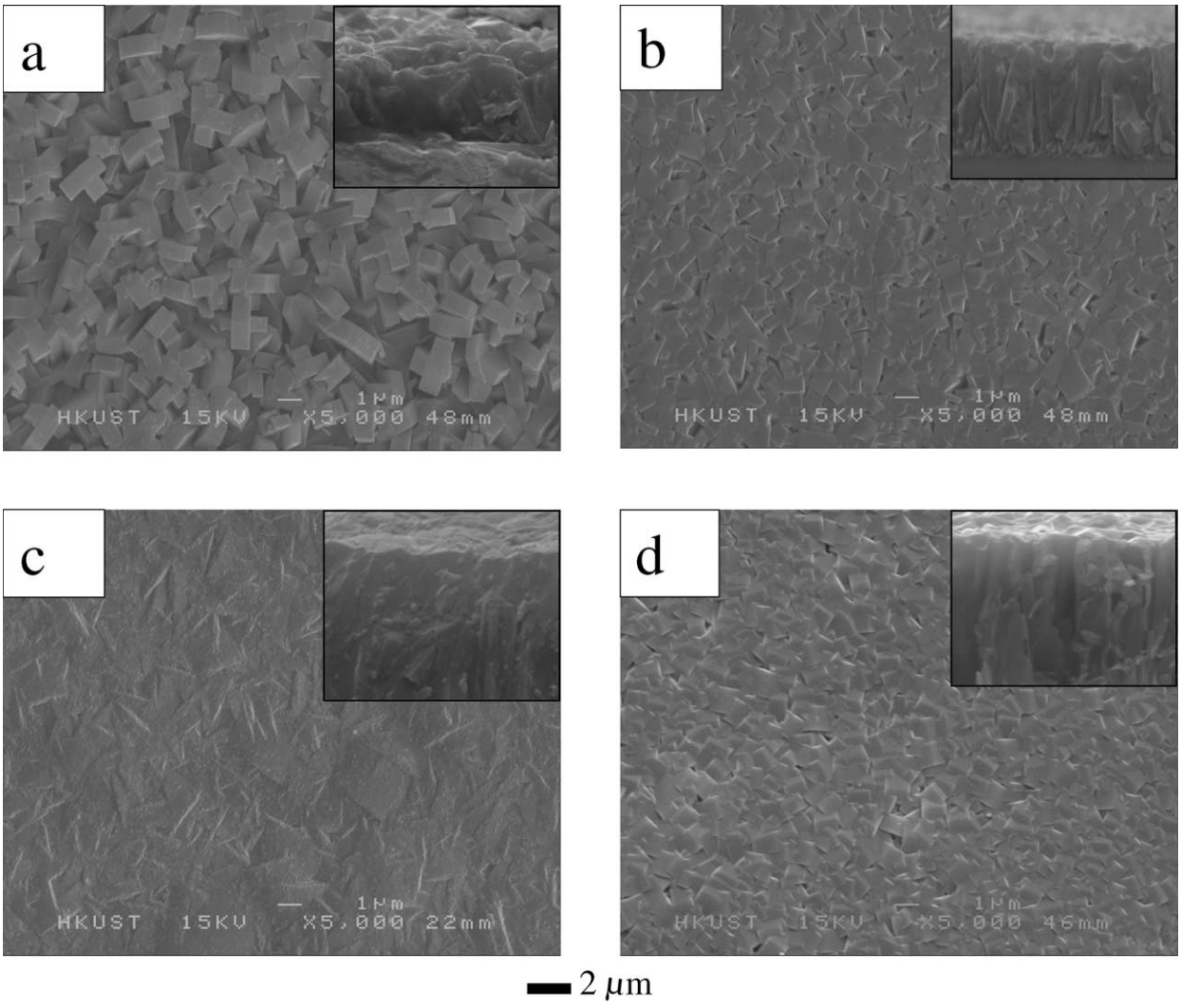

Fig. 6. MFI zeolites grown on silicon with seed populations of: (a) 1.5×10^{12} seeds/m^2 [40 TEOS:10 TPAOH:20,000 H_2O, 398 K], (b) 25×10^{12} seeds/m^2 [40 TEOS:10 TPAOH:20,000 H_2O, 398 K], (c) 95×10^{12} seeds/m^2 [40 TEOS:10 TPAOH:40 H_3BO_3:20,000 H_2O, 403 K, $t = 48$ h] and (d) 95×10^{12} seeds/m^2 [40 TEOS:1 TPAOH:9 NaOH:20,000 H_2O, 403 K, $t = 48$ h] (the figure insets are the cross-sectional view at 2$\times$ higher magnification).

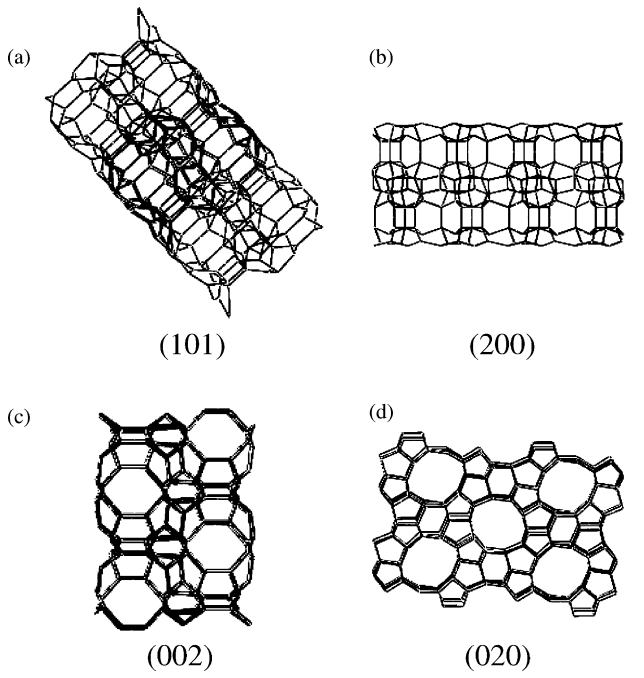

Fig. 7. Schematic drawing of the zeolite pore structure viewed along: (a) ⟨1 0 1⟩, (b) ⟨2 0 0⟩, (c) ⟨0 0 2⟩ and (d) ⟨0 2 0⟩ axes.

the film a preferred (2 0 0) orientation as indicated by the XRD pattern shown in Fig. 4e. In powder zeolite, the addition of boron results in ZSM-5 zeolites with cubic or spherical morphology instead of elongated coffin-shaped crystals [43,45]. Potassium was reported to have similar effects as boron on the MFI zeolites [46]. Replacing most of the TPA^+ ions with Na^+ in the synthesis solution gave the zeolite film shown in Fig. 6d a preferred (0 0 2) orientation (cf. Fig. 4f). Similar result can be obtained without the addition Na^+ by simply elevating the synthesis temperature to above 448 K. Fig. 7a–d displays the schematic drawing of the zeolite pore structure viewed along the ⟨1 0 1⟩, ⟨2 0 0⟩, ⟨0 0 2⟩ and ⟨0 2 0⟩ axes, respectively. Only the (0 2 0)-oriented film has the straight channel pores aligned normal to the silicon substrates, whereas in the other three orientations, the zigzag channel is normal to the support.

3.2. Fabrication of zeolite micropatterns and their stability

The previous section showed that zeolite films of controlled orientations (i.e., (1 0 1), (2 0 0) and (0 0 2)) and thickness could be grown on a silicon wafer to serve as substrate for the fabrication of microchemical devices. The ability to engineer and tailor the zeolite microstructure and chemistry is very important for the effective incorporation of zeolites as catalyst, membrane and structural materials in microchemical systems. The zeolite–silicon composite substrates were thermally stable, as they were able to withstand temperatures up to 873 K in both oxidising and reducing atmospheres for extended period of time without crack formation or film delamination. The zeolite film was also stable at room temperature in low to moderate concentrations of acids and bases (pH 3–10), except in the presence of fluoride containing acids and salts. However, corrosion of the silicon was evident in alkaline solution at a higher temperature (i.e., 353 K). The composite substrate was also stable in alcohol, acetone and aromatic solutions (e.g., xylene). However, this does not necessarily mean that the fabricated zeolite *micropatterns* are stable under similar conditions.

3.2.1. Zeolite microchannels

Fig. 8 displays three test patterns etched onto the zeolite–silicon composite substrate using the procedure discussed in Section 2. These images were taken after the microfabricated patterns had been subjected to 2 weeks of thermal cycling between 303 and 873 K in a furnace (∼40 K/min). Fig. 8a displays a series of microchannels etched onto a 10 μm thick Sil-1 (1 0 1) film grown on seeded silicon. The cross-section of the channels was rectangular with width of 5 μm. The shape of the serpentine channels was based on a cosine function with a periodicity defined by the peak-to-peak distance (L) of 15 μm. The shape of the channels was varied by changing the amplitude (A) of the cosine function. Starting from the left of the figure, the value of A for the first channel was 5 μm, the next two were 6 μm and the following two were 6.5 μm. The last two patterns consisted of staggered lines of 6 μm holes. It is clear from the results that complex microchannel geometry can be faithfully reproduced from the mask onto the zeolite–silicon composite substrate using the new fabrication technique. The pattern shown in Fig. 8b simulates a complex channel network that can exist in a microfluidic device. The figure shows a central distribution hub from which a network of microchannels radiates. Abrupt changes in channel width and direction were also incorporated to further test the precision of the new fabrication technique. The narrowest channel had a width of 3 μm and height of 10 μm, giving the channel an aspect ratio of about 3. There was no serious degradation in the microfabricated patterns (cf. Fig. 8a and b) even after prolonged exposure to harsh thermal conditions. Although microchannels narrower than 30 μm are rarely used in microchemical and microfluidic devices, the ability to fabricate high-resolution features is useful for incorporating microfabricated zeolite catalysts within microreactor channels.

3.2.2. Zeolite micropatterns

It had been demonstrated that catalytic zeolite powders and films can be incorporated in microchannels [15]. The microstructure of the catalyst coating could be engineered during the synthesis to introduce surface roughness and create intercrystalline porosity to promote fluid mixing and enhance mass transfer. Access to the zeolite can also be manipulated by changing the zeolite orientation (cf. Fig. 7). The zeolite deposited within the microchannels can be further micropatterned to create regular array of microfabricated

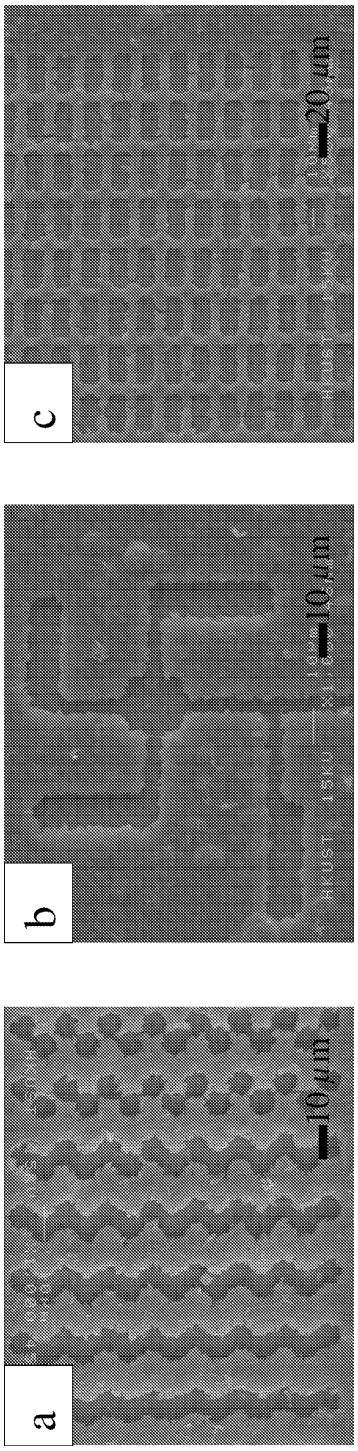

Fig. 8. Examples of zeolite micropatterns: (a) microchannel, (b) fluid distribution hub and (c) microfabricated grid.

catalysts with exact size, geometry and spacing. Fig. 8c shows an example of a microfabricated zeolite grid. Each line of zeolites forming the $8 \times 16\,\mu m^2$ rectangular grids was 5 μm wide and 10 μm high. The zeolite grid was stable during thermal treatment, and the occasional breaks in the zeolite lines were created during the etching process. Unlike fixed bed catalytic reactor, a microfabricated catalyst laid out in a regular pattern can be easier to simulate. Thus, an optimum catalyst array can be pre-designed to the specifications demanded by the application. Complex catalyst arrays can be fabricated with features as small as 3 μm using the new fabrication protocol. Further improvement in the fabrication procedure is underway to reach the target size of 1.25 μm, which is the current limit for photolithography. Electron beam lithography can create submicron features of about 0.1 μm [28], but the process is expensive and time consuming.

3.3. Incorporation of zeolites in microchemical devices

3.3.1. Zeolite-based microreactors

A variety of designs for microreactors have been suggested so far, but in all cases, the microchannel is the central structural element in the reactor architecture. The T-shaped microreactor used by Srinivasan et al. [47] is a simple yet elegant design. Based on a T-mixer, it allows in situ mixing of reactant streams (at a T-junction) before entering the reactor channel. Hsing et al. [48] have conducted both mathematical modelling and reaction experiments on the T-shaped microreactor, clearly demonstrating the effectiveness of the reactor design for many partial oxidation reactions. Fig. 9a displays a T-shaped microchannel etched onto a layer of (1 0 1)-oriented zeolite film supported on seeded silicon. The width of reactor microchannel was 500 μm and its length was 20 mm. The height of the channel is defined by the thickness of the zeolite film that forms the walls of the channel. Zeolite films that were less than a micron to more than 100 μm thick were prepared by varying the synthesis parameters. Fig. 10 displays three (1 0 1)-oriented zeolite–silicon composites with thicknesses of 1, 10 and 60 μm used in the study. These were prepared on seeded silicon using the synthesis composition and conditions summarised in Table 1. A magnified portion of the microchannel (Fig. 9b) clearly shows that the bottom of the channel is zeolite-free and the catalysis can take place mainly on the zeolite walls. Besides its role as catalyst, the zeolite also functions as the main structural material for the microreactor. One possible drawback in this reactor design is the molecular diffusion into the

Table 1
Synthesis composition and hydrothermal treatment conditions for Sil-1 zeolite composite shown in Fig. 11

	Synthesis mixture molar ratio	Temperature (K)	Time (h)
(a)	40 TEOS:10 TPAOH:20,000 H_2O	393	12
(b)	40 TEOS:10 TPAOH:20,000 H_2O	463	48 × 2
(c)	80 TEOS:10 TPAOH:20,000 H_2O	463	48 × 3

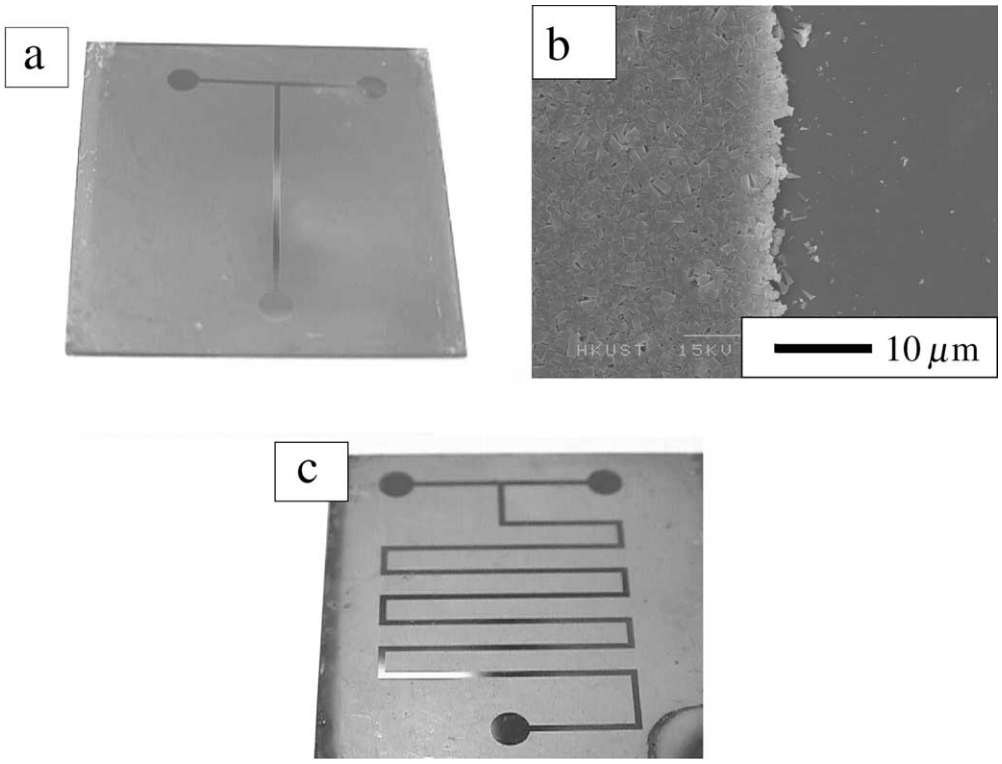

Fig. 9. (a) T-shaped microchannel etched onto a (1 0 1)-oriented Sil-1–silicon composite, (b) magnified view of the zeolite microchannel and (c) an example of serpentine-shape zeolite-based microreactor.

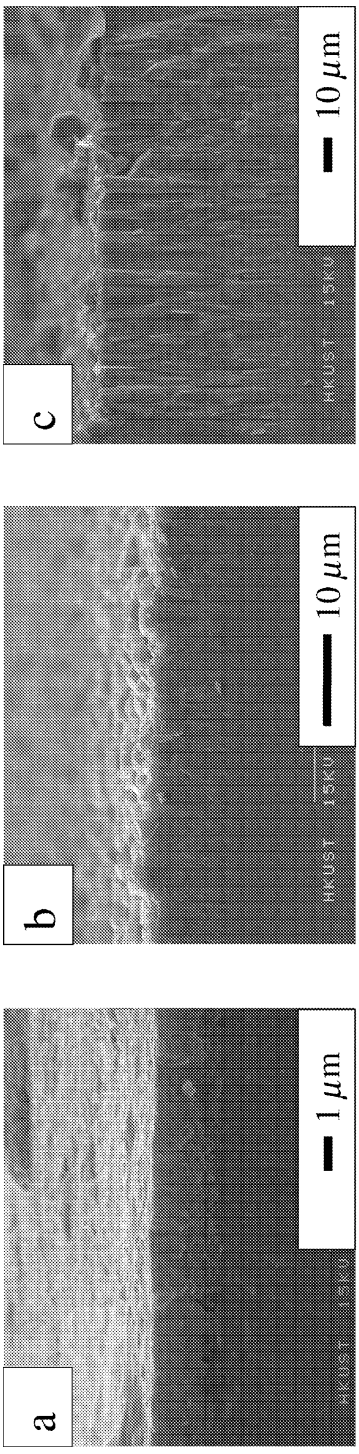

Fig. 10. Scanning electron micrographs of: (a) 1 μm, (b) 10 μm and (c) 60 μm thick zeolite–silicon composites.

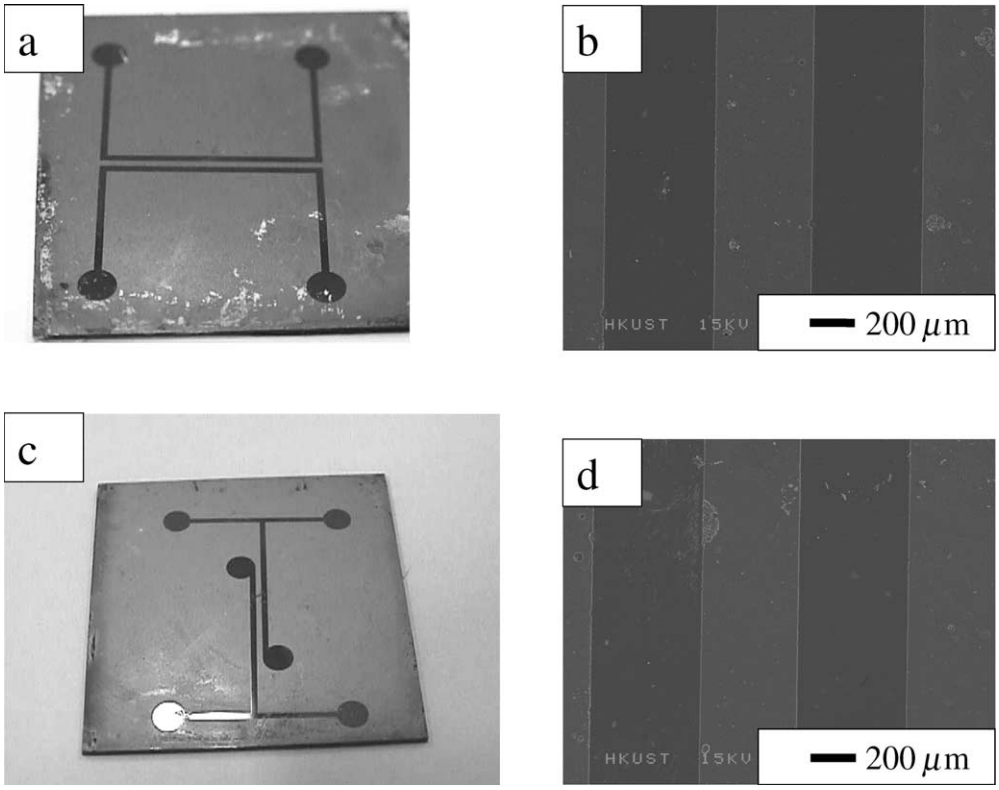

Fig. 11. (a) Design of a Sil-1 membrane microcontactor and (b) a magnified view of the membrane layer between two microchannels. (c) An I-shaped pattern fabricated onto Sil-1–silicon composite and (d) a magnified view of the membrane layer between the two microchannels.

bulk of the zeolite. This can pose a problem in various cases, such as in reaction rate determination. However, most molecules diffuse slowly in zeolite and for pentene and hexene, it will require a residence time greater than an hour to result in a 0.001% reactant loss in this type of microreactor design. A variation of the T-shaped microreactor design is shown in Fig. 9c. The main purpose of the serpentine structure is to provide longer residence time to accommodate reactions with slow kinetics.

3.3.2. Zeolite micromembranes

Zeolite with its uniform nanometer-sized pores and molecular sieving properties are ideal material for micromembranes. Zeolite membrane microseparator can serve many separation functions envisaged in a micro-analytical laboratory and miniature plant, from sample purification to product isolation. Fig. 11a displays a simple design for a miniature membrane contactor based on a Wicke–Kallenbach cell. The zeolite membrane between the two microchannels (Fig. 11b) would allow the selective exchange of components between two passing streams of liquid or gas. Using Sil-1 zeolite as the membrane barrier, hydrophobic compounds can be transferred across the membrane from an aqueous to an organic solution [49]. Molecular sieving separation of isomers and close-boiling compounds has been demonstrated in a Sil-1 membrane [50,51]. Similar separation performance is expected in a zeolite membrane microseparator. Unlike other chemical engineering unit operations, membrane scale down is straightforward and beneficial. It reduces the risks of failure in brittle inorganic membranes such as zeolites.

Membranes are integral part of many electrochemical and sensor devices [52], where permselective and semipermeable membranes are important. A permselective membrane allows the passage of a single type of ions or compounds, whereas a semipermeable membrane selectively excludes specific ions and molecules. Zeolite with its uniform, nanometer-sized pores and molecular sieving properties can find applications in these devices. For sensor applications, the zeolite membrane can enhance the sensor performance by acting as a selective barrier and by protecting the sensor elements from poisons and contaminants [53]. Fig. 11c shows one possible design for incorporating zeolite membrane in an electrochemical cell and sensor. The I-shaped pattern fabricated onto the zeolite film consists of four entry ports: two are for the electrodes and two are for fluid inlets. Two exit ports are available to allow for continuous flow of electrolyte solution or reactant gases (i.e., fuel cell). Fig. 11d shows that the two 400 μm channels are separated by a 300 μm zeolite membrane barrier. This thickness is comparable to that of a typical glass electrode [52,54]. However, zeolite membranes as thin as 5 μm can be fabricated if needed, using the new technique (cf. Fig. 8a).

4. Concluding remarks

A new fabrication procedure for incorporating zeolite catalysts, membranes and structural materials within the architecture of microchemical devices was developed based on microelectronic fabrication and zeolite thin film technologies. The ability to engineer and tailor the zeolite structure is essential for the incorporated zeolites to effectively perform its various tasks. Zeolite films with preferred orientation and engineered microstructure were successfully grown on silicon substrate. Direct manipulation of the film microstructure (i.e., thickness, orientation, etc.) was achieved by controlling the seed population, synthesis composition and hydrothermal treatment conditions. High-resolution micropatterns of complex microchannel network and geometry, as well as, particle arrays were successfully fabricated from zeolite. These zeolite patterns survived prolonged thermal treatment under harsh conditions (i.e., temperature oscillation between 303 and 873 K) demonstrating their excellent thermal stability. Design blueprints for the incorporation of zeolites in microreactors, membrane microseparators and microelectrochemical cell were presented. Working models were built using the new fabrication technique, and the structural details of the microsystem architecture were examined. Studies are now underway to test the performance of the zeolite-based microchemical devices for chemical reactions and separations.

Acknowledgements

We gratefully acknowledge the Hong Kong Research Grant Council (HKUST 6021/01P) and Institute of Nano Science and Technology (INST) for funding this research. Y.S.S. Wan also thanks the Croucher Foundation for her scholarship. We also acknowledge the technical support provided by the Microelectronics Fabrication Facility (MFF) and Materials Characterization and Preparation Facility (MCPF) of the Hong Kong University of Science and Technology (HKUST).

References

[1] J.C. Jansen, D. Kascchiev, A. Erdem-Senatalar, Preparation of coating of molecular sieve crystals for catalysis and separation, in: J.C. Jansen, M. Stöcker, H.G. Karge, J. Weitkamp (Eds.), Advanced Zeolite Science and Applications, Studies in Surface Science and Catalysis, Vol. 85, Elsevier, Amsterdam, 1994, pp. 215–250.

[2] I.E. Maxwell, W.H.J. Stork, Hydrocarbon processing with zeolites, in: H. van Bekkum, E.M. Flanigen, J.C. Jansen (Eds.), Introduction to Zeolite Science and Practice, Studies in Surface Science and Catalysis, Vol. 58, Elsevier, Amsterdam, 1991, pp. 571–630.

[3] W.F. Hölderich, H. van Bekkum, Zeolites in organic synthesis, in: H. van Bekkum, E.M. Flanigen, J.C. Jansen (Eds.), Introduction to Zeolite Science and Practice, Studies in Surface Science and Catalysis, Vol. 58, Elsevier, Amsterdam, 1991, pp. 631–726.

[4] E.G. Derouane, G. Crehan, C.J. Dillon, D. Bethell, H. He, S.B. Derouane-Abd Hamid, Zeolite catalysts as solid solvents in fine chemicals synthesis. 2. Competitive adsorption of the reactants and products in the Friedel–Crafts acetylations of anisole and toluene, J. Catal. 194 (2000) 410–423.

[5] Y. Nishizaka, M. Misono, Catalytic reduction of nitrogen monoxide by methane over palladium-loaded zeolites in the presence of oxygen, Chem. Lett. (1993) 1295–1298.

[6] S. Sato, Y. Yu-u, H. Yahiro, N. Mizuno, M. Iwamoto, Cu-ZSM-5 zeolite as highly active catalyst for removal of nitrogen monoxide from emission of diesel engines, Appl. Catal. 70 (1991) L1–L5.

[7] J. Coronas, J. Santamaria, Separations using zeolite membranes, Sep. Purification Meth. 28 (1999) 127–177.

[8] D. Casanave, A. Giroir-Fendler, J. Sanchez, R. Loutaty, J.-A. Dalmon, Control of transport properties with a microporous membrane reactor to enhance yields in dehydrogenation reactions, Catal. Today 25 (1995) 309–314.

[9] J. Coronas, J. Santamaria, Catalytic reactors based on porous ceramic membranes, Catal. Today 51 (1999) 377–389.

[10] W. Göpel, T.A. Jones, M. Kleitz, J. Lundström, T. Seiyama, Sensors: A Comprehensive Survey, Vol. 2, Chemical and Biochemical Sensors, Part I, VCH, Weinheim, 1991, pp. 207–225.

[11] Y. Yan, T. Bein, Zeolite thin film with tunable molecular sieve function, J. Am. Chem. Soc. 117 (1995) 9990–9994.

[12] Y. Yan, T. Bein, Molecular recognition on acoustic wave devices: sorption in chemically anchored zeolite monolayers, J. Phys. Chem. 96 (1992) 9387–9393.

[13] L. Scandella, G. Binder, T. Mezzacasa, J. Gobrecht, R. Berger, H.P. Lang, Ch. Gerber, J.K. Gimezewski, J.H. Koegler, J.C. Jansen, Combination of single crystal zeolites and microfabrication: two applications towards zeolite nanodevices, Micropor. Mesopor. Mater. 21 (1998) 403–409.

[14] Ch. Striebel, K. Hoffmann, F. Marlow, Microcrystal prism method for refractive index measurements on zeolite-based nanocomposites, Micropor. Mater. 9 (1997) 43–50.

[15] Y.S.S. Wan, J.L.H. Chau, A. Gavriilidis, K.L. Yeung, Design and fabrication of zeolite-based microreactors and microseparators, Micropor. Mesopor. Mater. 42 (2001) 157–175.

[16] W. Ehrfeld, V. Hessel, H. Löwe, Microreactors New Technology for Modern Chemistry, VCH, Weinheim, 2000.

[17] M.K. Drost, C.J. Call, J.M. Cuta, R.S. Wegeng, Microchannel integrated evaporator/combustor thermal process, J. Microscale Thermophys. Eng. 1 (1997) 321–332.

[18] W. Ehrfeld, Cl. Gärtner, K. Golbig, V. Hessel, R. Konrad, H. Löwe, Th. Richter, Ch. Schulz, Fabrication of components and systems for chemical and biological microreactors, in: Proceedings of the First International Conference on Microreaction Technology, Springer, Berlin, 1998, pp. 72–90.

[19] J. Brandner, M. Fichtner, U. Schygulla, K. Schubert, Improving the efficiency of micro-heat exchangers and reactors, in: Proceedings of the Fourth International Conference on Microreaction Technology, Atlanta, USA, 2000, pp. 244–249.

[20] W. Ehrfeld, V. Hessel, H. Löwe, Extending the knowledge base in microfabrication towards chemical engineering and fluid dynamics simulation, in: Proceedings of the Fourth International Conference on Microreaction Technology, Atlanta, USA, 2000, pp. 3–20.

[21] M.W. Losey, S. Isogai, M.A. Schmidt, K.F. Jensen, Microfabricated devices for multiphase catalytic processes, in: Proceedings of the Fourth International Conference on Microreaction Technology, Atlanta, USA, 2000, pp. 416–422.

[22] A.L.Y. Tonkovich, S.P. Fitzgerald, J.L. Zilka, M.J. LaMont, Y. Wang, D.P. VanderWiel, R.S. Wegeng, Microchannel chemical reactors for fuel processing applications. II. Compact fuel vaporization, in: Proceedings of the Third International Conference on Microreaction Technology: Industrial Prospects, Springer, Berlin, 2000, pp. 364–371.

[23] E. Dietzsch, D. Hönicke, M. Fichtner, K. Schubert, G. Wießmeier, The formation of cycloalkenes in the partial gas phase hydrogenation of *c,t,t*-1,5,9-cyclododecatriene, 1,5-cyclooctadiene and benzene in

microchannel reactors, in: Proceeding of the Fourth International Conference on Microreaction Technology, Atlanta, USA, 2000, pp. 89–99.
[24] W. Ehrfeld, V. Hessel, H. Lehr, Microreactors for chemical synthesis and biotechnology—current developments and future applications, in: A. Manz, H. Becker (Eds.), Microsystem Technology in Chemistry and Life Sciences, Springer, Berlin, 1998, pp. 233–252.
[25] A.J. Franz, K.F. Jensen, M.A. Schmidt, Palladium membrane microreactors, in: Proceedings of the Third International Conference on Microreaction Technology: Industrial Prospects, Springer, Berlin, 1999, pp. 267–276.
[26] M.J. den Exter, H. van Bekkum, C.J.M. Rijn, F. Kapteijn, J.A. Moulijn, H. Schellevis, C.I.N. Beenakker, Stability of oriented silicalite-1 films in view of zeolite membrane preparation, Zeolites 19 (1997) 13–20.
[27] N. Maluf, An Introduction to Microelectromechanical System Engineering, Artech House, USA, 2000, pp. 41–75.
[28] M. Madou, Fundamentals of Microfabrication, CRC Press, New York, 1997, pp. 38, 217–266.
[29] K.D. Wise, K. Najafi, Microfabrication techniques for integrated sensors and microsystems, Science 254 (1991) 1335–1342.
[30] H. Lehr, W. Ehrfeld, Advanced microstructure products by synchrotron radiation lithography, J. Phys. IV 4 (1994) 229–236.
[31] W. Ehrfeld, V. Hessel, H. Löwe, Ch. Schulz, L. Weber, Materials of LIGA technology, Microsyst. Technol. 5 (1999) 105–112.
[32] P.M. Martin, D.W. Matson, W.D. Bennett, Microfabrication methods for microchannel reactors and separations systems, in: Proceedings of the Second International Conference on Microreaction Technology, New Orleans, USA, 1998, pp. 75–80.
[33] D.W. Matson, P.M. Martin, D.C. Stewart, A.L.Y. Tonkovich, M. White, J.L. Zilka, G.L. Roberts, Fabrication of microchannel chemical reactors using a metal lamination process, in: Proceedings of the Third International Conference on Microreaction Technology: Industrial Prospects, Springer, Berlin, 1999, pp. 62–71.
[34] S. Johansson, J.-Å. Schweitz, H. Westberg, M. Boman, Microfabrication of three-dimensional boron structures by laser chemical processing, J. Appl. Phys. 72 (1992) 5956–5963.
[35] J. Arnold, U. Dasbach, W. Ehrfeld, K. Hesch, H. Löwe, Combination of excimer laser micromachining and replication processes suited for large scale production, Appl. Surf. Sci. 86 (1995) 251–258.
[36] R.D. Piner, J. Zhu, F. Xu, S.H. Hong, C.A. Mirkin, Dip-Pen nanolithography, Science 283 (1999) 661–663.
[37] J.C. Jansen, G.M. van Rosmalen, Oriented growth of silica molecular sieve crystals as supported films, J. Cryst. Growth 128 (1993) 1150–1156.
[38] M.C. Lovallo, A. Gouzinis, M. Tsapatsis, Synthesis and characterization of oriented MFI membranes prepared by secondary growth, AIChE J. 44 (1998) 1903–1913.
[39] K. Ha, Y.-J. Lee, Y.S. Chun, Y.S. Park, G.S. Lee, K.B. Yoon, Photochemical pattern transfer and patterning of continuous zeolite films on glass by direct dipping in synthesis gel, Adv. Mater. 13 (2001) 594–596.
[40] J. Sterte, S. Mintova, G. Zhang, B.J. Schoeman, Thin molecular sieve films on noble metal substrate, Zeolite 18 (1997) 387-390.
[41] J.L.H. Chau, T. Carlos, K.L. Yeung, K. Ho, The role of surface chemistry on zeolite membrane formation, J. Membr. Sci. 164 (2000) 257–275.
[42] T. Bein, Synthesis and applications of molecular sieve layers and membranes, Chem. Mater. 8 (1996) 1636–1653.
[43] J.C. Jansen, The preparation of molecular sieves: a synthesis of zeolites, in: H. van Bekkum, E.M. Flanigen, J.C. Jansen (Eds.), Introduction to Zeolite Science and Practice, Studies in Surface Science and Catalysis, Vol. 58, Elsevier, Amsterdam, 1991, pp. 77–136.
[44] A. Iwasaki, I. Kudo, T. Sano, Three-dimensional real-time observation of growth and dissolution of silicalite crystal, in: H. Chon, S.-K. Ihm, Y.S. Uh (Eds.), Progress in Zeolite and Microporous Materials, Studies in Surface Science and Catalysis, Vol. 105, Elsevier, Amsterdam, 1997, pp. 317–324.
[45] E.G. Derouane, S. Detremmerie, Z. Gabelica, N. Blom, Synthesis and characterization of ZSM-5 type zeolites. 1. Physicochemical properties of precursors and intermediates, Appl. Catal. 1 (1981) 201–224.
[46] Z. Gabelica, N. Blom, E.G. Derouane, Synthesis and characterisation of ZSM-5 type zeolites. 3. A critical-evaluation of the role of alkali and ammonium cation, Appl. Catal. 5 (1983) 227.
[47] R. Srinivasan, I.-M. Hsing, P.E. Berger, K.F. Jensen, S.L. Firebaugh, M.A. Schmidt, M.P. Harold, J.J. Lerou, J.F. Ryley, Micromachined reactors for catalytic partial oxidation reactions, AIChE J. 43 (1997) 3059–3069.
[48] I.-M. Hsing, R. Srinivasan, M.P. Harold, K.F. Jensen, M.A. Schmidt, Simulation of micromachined chemical reactors for heterogeneous partial oxidation reactions, Chem. Eng. Sci. 55 (2000) 3–13.
[49] S. Wu, C. Bouchard, S. Kaliaguine, Zeolite containing catalytic membranes as interphase contactors, Res. Chem. Intermed. 24 (1998) 273–280.
[50] H.H. Funke, A.M. Argo, C.D. Baertsch, J.L. Falconer, R.D. Noble, Separation of close-boiling hydrocarbons with silicalite zeolite membranes, J. Chem. Soc., Faraday Trans. 92 (1996) 2499.
[51] H.H. Funke, M.G. Kovalchick, J.L. Falconer, R.D. Noble, Separation of hydrocarbon isomer vapors with silicalite zeolite membranes, Ind. Eng. Chem. Res. 35 (1996) 1575.
[52] J. Janata, Principles of Chemical Sensors, Plenum Press, New York, 1989, p. 81.
[53] O. Hugon, M. Sauvan, P. Benech, C. Pijolat, F. Lefebvre, Gas separation with a zeolite filter, application to the selectivity enhancement of chemical sensors, Sensors Actuators B 67 (2000) 235–243.
[54] A.A. Belyustin, Silver ion response as a test for the multilayer model of glass electrodes, Electroanalysis 11 (1999) 799–803.